Critical Level Statistics of the Fibonacci Model

Michihiro Naka[1], Kazusumi Ino[1] and Mahito Kohmoto[2]
[1]*Department of Pure and Applied Sciences, University of Tokyo, Komaba 3-8-1, Meguro-ku, Tokyo, 153-8902, Japan*
[2]*Institute for Solid State Physics, University of Tokyo, Kashiwanoha 5-1-5, Kashiwa-shi, Chiba, 277-8581, Japan*

We numerically analyze spectral properties of the Fibonacci model which is a one-dimensional quasiperiodic system. We find that the energy levels of this model have the distribution of the band widths w obeys $P_B(w) \sim w^\alpha$ $(w \to 0)$ and $P_B(w) \sim e^{-\beta w}$ $(w \to \infty)$, the gap distribution $P_G(s) \sim s^{-\delta}$ $(s \to 0)$ $(\alpha, \beta, \delta > 0)$. We also compare the results with those of multi-scale Cantor sets. We find qualitative differences between the spectra of the Fibonacci model and the multi-scale Cantor sets.

PACS numbers: 05.45.Pq, 05.70.Jk, 71.23.Ft

I. INTRODUCTION

Bloch's theorem tells that the free electron eigenstates are always extended in periodic systems. It is also well known that the free electron eigenstates are always localized in one-dimensional random media [1]. On the other hand, one-dimensional quasiperiodic systems show various interesting behavior [2]. A one-dimensional tight-binding model is

$$t_{i+1}\psi_{i+1} + t_{i-1}\psi_{i-1} + \epsilon_i\psi_i = E\psi_i, \tag{1}$$

where ψ_i denotes the value of the wave function at i-th site, t_i and ϵ_i are the hopping matrix element and the site energy at i-th site respectively, both of which can be taken to be quasiperiodic with lattice spacing. The Harper model: $t_i = 1$ and $\epsilon_i = \lambda\cos(2\pi\sigma i + \theta)$ has been well studied. When σ is an irrational number, it is quasiperiodic. The eigenstates of the quasiperiodic Harper model are extended for $\lambda < 2$ and are localized for $\lambda > 2$ with the metal-insulator transition point $\lambda = 2$ [3]. Hofstadter found a surprisingly rich structure of the spectrum at $\lambda = 2$ [4]. There the spectrum as well as the eigenstates become multifractal [2]. The total measure of the bands at the critical point is zero with a fractal dimension less than one [5, 6]. The scaling behavior of the spectrum has been extensively studied [2] by multifractal analysis [7].

Recently a new statistical characterization of the spectrum of the Harper model at the critical point was found [8, 9]. The distribution of the normalized width of the bands was examined. The distribution of the bandwidths $P_B(w)dw$ counts the number of bands whose values are between w and $w + dw$. In [8], $P_B(w)$ was numerically investigated at $\lambda = 2$ and $\sigma = \frac{\sqrt{5}-1}{2}$ and it was claimed that $P_B(w)$ follows the semi-Poissonian distribution $4we^{-2w}$. However this claim has been excluded by further detailed numerical investigations [9]. Still it has been confirmed that

$$P_B(w) \sim w^\alpha \quad (w \to 0), \tag{2}$$

and

$$P_B(w) \sim e^{-\beta w} \quad (w \to \infty), \tag{3}$$

where $\alpha \sim 2.5, \beta \sim 1.4$ [9]. Similar laws are also found for a variant of the Harper model at its criticality [9].

For the Harper model, the distribution of energy gaps $P_G(s)$ was also examined. The distribution diverges near the origin and follows an inverse power law [9, 10]

$$P_G(s) \sim s^{-\delta} \quad (s \to 0), \tag{4}$$

with $\delta \sim 1.5$. This law is also extended to a variant of the Harper model [9].

In order to investigate how these laws are universal for critical quasiperiodic systems, we study the one-dimensional Fibonacci model [11, 12]. It is a model obtained by setting t_i or ϵ_i in (1) to the Fibonacci sequence. We shall study the case with $\epsilon_i = 0$. The Fibonacci model remains critical when varying the parameters t_i, and the spectra are multifractal similar to that at the critical point $\lambda = 2$ of the Harper model [2]. We will find qualitatively similar but quantitatively different behavior of $P_B(w)$ and $P_G(s)$.

A remarkable feature of this model is that the construction of the Fibonacci sequence can be translated to a renormalization group transformation, and its action on the trace of the transfer matrix becomes a nonlinear dynamical system called the Kohmoto-Kadanoff-Tang (KKT) map[11]. The KKT map has been analyzed as a nonlinear dynamical system [13, 14, 15]. Namely the periodic orbit corresponding to the bands' center was analyzed, and the scaling property of the band was shown to be determined by the eigenvalues of the linearized map at the hyperbolic points. They induce heteroclinic points of the KKT map. The structure of subsets of the spectrum was explained by the Smale's horseshoe structure. This analysis can be extended to other bands and then the explanation is generalized to a subset of the whole spectrum [15].

The Smale's horseshoe structure indicates that the spectrum of the Fibonacci model is a multi-scale Cantor set. Here, we restrict the meaning of the term "multi-scale Cantor set" as the set which is obtained by the

following procedure : we transform the interval $I = [0, 1]$ into a finite number of subintervals with definite scales and apply the transformation to subintervals successively. In the literature, the term "Cantor set" is also used as the term for "a closed set with no isolated points and whose complement is dense". We call this "general Cantor set". We will compare our results with those of multi-scale Cantor sets. Also note that the spectrum of the Fibonacci model is proved to be singular continuous [16]. Nevertheless the comparison will turn out to be useful.

In Sec.II, we recall the renormalization group transformation. In Sec.III, we report the results of our numerical studies. In Sec.IV, we compare our results with those of multi-scale Cantor sets. Sec.V gives conclusion. In Appendix, we provide definition and distributions of multi-scale Cantor sets.

II. FIBONACCI MODEL AND THE KOHMOTO-KADANOFF-TANG MAP

We recall the aspects of the Fibonacci model we use, especially the renormalization group transformation [11].

The Fibonacci model describes a one-dimensional quasiperiodic system given by (1) with $\epsilon_i = 0$, defined by

$$t_{i+1}\psi_{i+1} + t_i\psi_{i-1} = E\psi_i, \tag{5}$$

where t_i's take two values t_a and t_b arranged in the Fibonacci sequence constructed recursively as $S_{\ell+1} = \{S_\ell, S_{\ell-1}\}$ $(\ell \geq 1)$ with an initial condition $S_0 = \{b\}, S_1 = \{a\}$. The number of elements in S_ℓ is the Fibonacci number F_ℓ defined by $F_{\ell+1} = F_\ell + F_{\ell-1}$ $(\ell \geq 1)$ with an initial condition $F_0 = F_1 = 1$. To investigate the model with infinite sites, one considers a finite size system of (5) with F_ℓ sites and imposes a boundary condition on the states. Then the system is equivalent to the system with a period F_ℓ.

We write Eq.(5) as

$$\begin{pmatrix} \psi_{i+1} \\ \psi_i \end{pmatrix} = \begin{pmatrix} \frac{E}{t_{i+1}} & -\frac{t_i}{t_{i+1}} \\ 1 & 0 \end{pmatrix} \begin{pmatrix} \psi_i \\ \psi_{i-1} \end{pmatrix}. \tag{6}$$

The present 2×2 matrix is a transfer matrix. Values of the wave function at any lattice sites are related to those of the initial sites by applying the transfer matrices successively. There are three types of transfer matrices :

$$M_{aa} = \begin{pmatrix} \frac{E}{t_a} & -1 \\ 1 & 0 \end{pmatrix},$$
$$M_{ab} = \begin{pmatrix} \frac{E}{t_a} & -\frac{t_b}{t_a} \\ 1 & 0 \end{pmatrix}, \quad M_{ba} = \begin{pmatrix} \frac{E}{t_b} & -\frac{t_a}{t_b} \\ 1 & 0 \end{pmatrix}. \tag{7}$$

We introduce a matrix M_ℓ which generates a wave function at the F_ℓ-th site

$$\begin{pmatrix} \psi_{F_\ell+1} \\ \psi_{F_\ell} \end{pmatrix} = M_\ell \begin{pmatrix} \psi_1 \\ \psi_0 \end{pmatrix}. \tag{8}$$

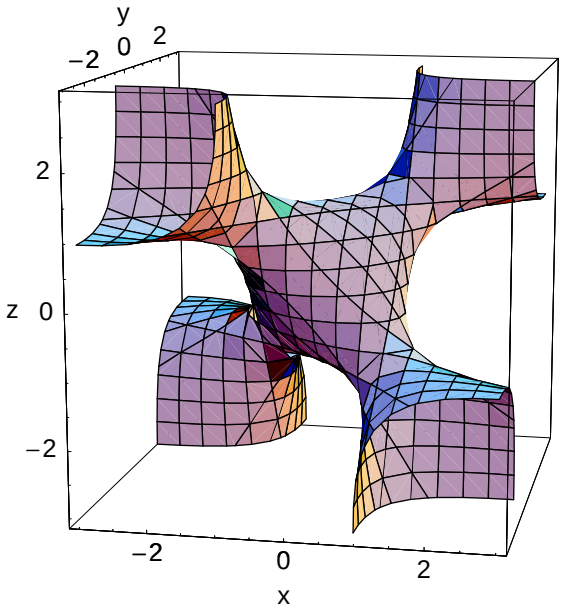

FIG. 1: Two-dimensional manifold $x^2+y^2+z^2-2xyz-1 = I$ for $I = \frac{9}{16}$. The manifold consists of a central body and four parts to infinity. The four parts are connected to the central body through four tubes.

This matrix M_ℓ is given by a successive product of the transfer matrices, and the number of element of the product is F_ℓ which grows like $\sigma^{-\ell}$. A special property of the transfer matrices of the Fibonacci model is that M_ℓ is determined by a recursive map [11]

$$M_{\ell+1} = M_{\ell-1}M_\ell, \tag{9}$$

with an initial condition $M_1 = M_{aa}, M_2 = M_{ab}M_{ba}$. This map simplifies a procedure to obtain the matrix M_ℓ.

As M_ℓ's are unimodular matrices, using the trace of the matrix M_ℓ, the equation (9) is casted to

$$x_{\ell+1} = y_\ell, \quad y_{\ell+1} = z_\ell, \quad z_{\ell+1} = 2y_\ell z_\ell - x_\ell, \tag{10}$$

where $x_\ell = \frac{1}{2}\mathrm{Tr}M_\ell$ and we introduce three-dimensional vectors $\vec{r}_\ell = (x_\ell, y_\ell, z_\ell) = (x_\ell, x_{\ell-1}, x_{\ell-2})$ [11]. This map $\vec{r}_{\ell+1} = f(\vec{r}_\ell)$ is the KKT map. An initial condition is $x_1 = \frac{E}{2t_a}, y_1 = \frac{E}{2t_b}, z_1 = \frac{1}{2}\left(\frac{t_b}{t_a} + \frac{t_a}{t_b}\right)$. It is remarkable that this map has a constant of motion [13]:

$$I = x_\ell^2 + y_\ell^2 + z_\ell^2 - 2x_\ell y_\ell z_\ell - 1. \tag{11}$$

The initial condition gives the value of this constant of motion as

$$I = \frac{1}{4}\left(\frac{t_b}{t_a} - \frac{t_a}{t_b}\right)^2. \tag{12}$$

The constant of motion I determines a two-dimensional manifold on which an orbit of the KKT map remains. In Fig. 1, an example of the manifold is shown. It is always non-compact as long as $I > 0$. When I approaches

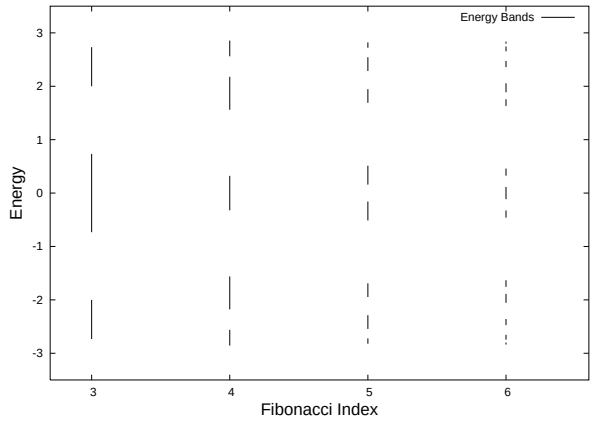

FIG. 2: Energy bands at $(t_a, t_b) = (1, 2)$, $I = \frac{9}{16}$ with Fibonacci numbers $F_3 = 3, F_4 = 5, F_5 = 8$ and $F_6 = 13$. The bands consist of F_ℓ bands and $F_\ell - 1$ gaps.

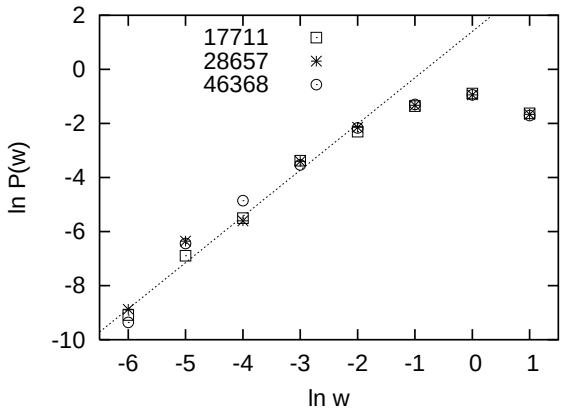

FIG. 3: Band-width distributions at $(t_a, t_b) = (1, 2)$, $I = \frac{9}{16}$. The distributions for $\ln w < 1.5$ suggest $P_B(w) \sim w^{1.71}$.

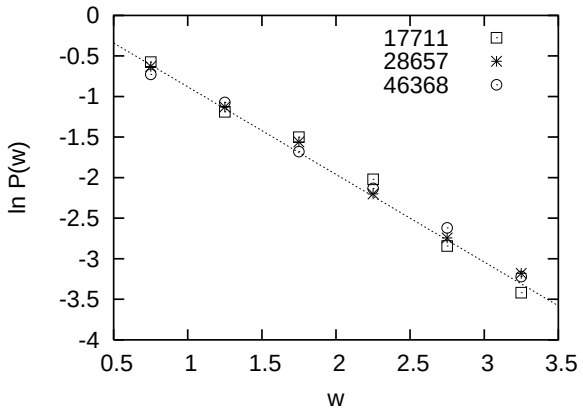

FIG. 4: Band-width distributions with w-$\ln P_B(w)$ plots at $(t_a, t_b) = (1, 2)$, $I = \frac{9}{16}$. The distributions for $w > 0.5$ suggest $P_B(w) \sim e^{-1.08w}$.

zero, the tubes shrink to points. A case $I < 0$ does not represent the electronic systems.

In Fig. 2, we show the energy bands for small ℓ's. Since the eigenstates of the model must be normalizable, we impose the condition on the initial condition so that $|\psi_{F_\ell}|$ does not grow exponentially. In other words, the energy levels of the equation (5) with F_ℓ is determined by the condition $|x_\ell| \leq 1$ since the energy enters in the initial condition of the KKT map. It can also be shown that a condition $|x_i|, |x_{i+1}| > 1$ for an $i < \ell$ is sufficient for the corresponding energy to be in an energy gap. For large F_ℓ, the KKT map provides escaping orbits on the manifold for almost all energies and the remaining set is shrinking to zero measure as $F_\ell \to \infty$.

III. LEVEL STATISTICS

We use the KKT map described in the previous section to get the spectrum of the Fibonacci model. We first consider periodic systems whose unit cell is a Fibonacci number F_ℓ, then extrapolate results to understand the Fibonacci model $\ell = \infty$.

Let us begin with the band-width distribution $P_B(w)$. We normalize the distribution by $\int_0^\infty P_B(w)dw = 1$ and $\int_0^\infty wP_B(w)dw = 1$. Each band width approaches zero at limit $\ell \to \infty$ [14, 15]. At a finite Fibonacci index ℓ, we normalize the band widths by the mean of them and consider distribution $P_B^{(\ell)}(w)$ of the normalized band widths. Then we extrapolate $P_B(w)$ at $\ell \to \infty$.

Fig. 3 shows $\ln w$-$\ln P_B(w)$ plots. As $w \to 0$, the distribution $P_B(w)$ converges to zero. The results for different ℓ seems to be on the same line, which suggests the existence of band-width distribution at $\ell \to \infty$. The distribution $P_B(w)$ takes a form

$$P_B(w) \sim w^\alpha \qquad (w \to 0), \tag{13}$$

with a positive real number α. This form remains to hold when I changes. The values of α for several cases are given in Table I.

We next consider a region where w is larger than 0.5. In Fig. 4, we present distribution in w-$\ln P_B(w)$ plots. The linear behavior suggests that the distribution $P_B(w)$ at large w is given by a form

$$P_B(w) \sim e^{-\beta w} \qquad (w \to \infty), \tag{14}$$

with a positive real number β. Estimated values of β for several cases are presented in Table I. We have changed the hopping coefficients t_a and t_b for fixed I's for several cases. The results indicate that α and β depend on t_a and t_b only through the value of I.

Next we examine the ansatz that the distribution $P_B(w)$ is described by a combined distribution $P(w) = N_{\alpha\beta} w^\alpha e^{-\beta w}$ with a normalization constant $N_{\alpha\beta}$ for every value of w. This is the semi-Poisson form as was assumed for the Harper model [8]. The normalization conditions

t_a	t_b	I	α	β	δ
$\frac{11}{8}$	$\frac{13}{8}$	$\frac{576}{20449}$	1.20(±0.03)	0.38(±0.08)	0.935(±0.004)
$\frac{5}{4}$	$\frac{7}{4}$	$\frac{144}{1225}$	1.28(±0.05)	1.05(±0.08)	0.824(±0.004)
$\frac{9}{8}$	$\frac{15}{8}$	$\frac{64}{225}$	1.42(±0.07)	1.07(±0.07)	0.747(±0.004)
1	2	$\frac{9}{16}$	1.71(±0.07)	1.08(±0.06)	0.689(±0.004)
$\frac{7}{8}$	$\frac{17}{8}$	$\frac{14400}{14161}$	1.87(±0.13)	1.18(±0.07)	0.612(±0.002)
$\frac{3}{4}$	$\frac{9}{4}$	$\frac{16}{9}$	1.91(±0.09)	1.29(±0.08)	0.555(±0.003)
$\frac{5}{8}$	$\frac{19}{8}$	$\frac{28224}{9025}$	2.23(±0.17)	1.50(±0.12)	0.490(±0.002)

TABLE I: Estimated values for critical indices α, β and δ. Errors arise in fitting numerical data to the proposed distributions.

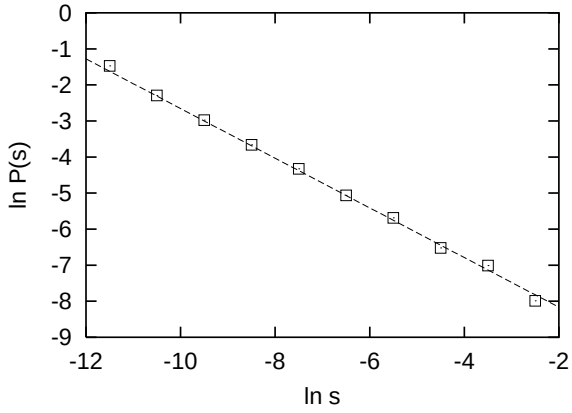

FIG. 5: Gap distribution $\ln s$-$\ln P_G(s)$ for $(t_a, t_b) = (1, 2)$, $I = \frac{9}{16}$ and $F_{21} = 17711$. $P_G(s) \sim s^{-0.689}$.

for the band-width distribution impose the relation between the indices $\beta = \alpha + 1$. Then the distribution reduces to generalized form of the semi-Poisson distribution $P(w) = \frac{(\alpha+1)^{\alpha+1}}{\Gamma(\alpha+1)} w^\alpha e^{-(\alpha+1)w}$. However this is different from the obtained behavior at $w \to 0, \infty$. Thus we exclude the ansatz of the semi-Poisson distribution.

We found that the gap distribution $P_G(s)$ always diverge for $s \to 0$. An example using the $\ln s$-$\ln P_G(s)$ plot is shown in Fig. 5. We normalize the distribution as $\int_0^\infty P_G(s)ds = 1$. From Fig. 5, the gap distribution obeys an inverse power law

$$P_G(s) \sim s^{-\delta} \qquad (s \to 0), \tag{15}$$

which diverges at the origin. Values of δ for several cases are given in Table I. We have changed the hopping coefficients t_a and t_b for fixed I's for several cases. The results indicate that δ depends on t_a and t_b only through I.

IV. COMPARISON WITH THE MULTI-SCALE CANTOR SETS

We compare our results in the previous section with properties of multi-scale Cantor sets which are produced

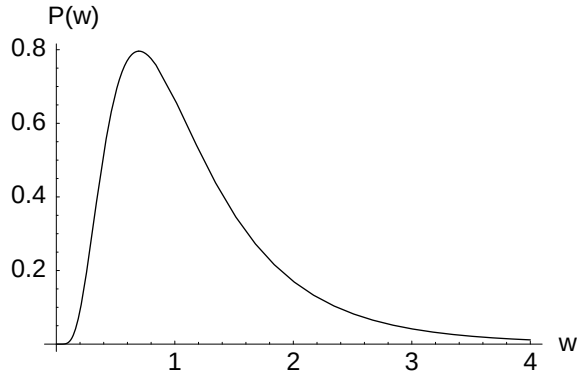

FIG. 6: Logarithmic normal distribution $P(w) = \frac{1}{w} N_{(\mu,\sigma^2)}(\ln w) = \frac{1}{\sqrt{2\pi}\sigma} \frac{1}{w} e^{-\frac{(\log w - \mu)^2}{2\sigma^2}}$ with $\mu = 0, \sigma = 0.6$

by splitting an interval into a definite number of subintervals with definite scales (see Appendix for details). We call the intervals of the multi-scale Cantor sets "bands", while we call the removed intervals as "gaps".

Let us consider the band-width distribution of a multi-scale Cantor set, $P_B^{(\mathrm{Cantor})}(w)$. As far as we know, $P_B^{(\mathrm{Cantor})}(w)$ has not been appeared in the literature. However, Kolmogorov's theory of turbulence [17] introduces the energy distribution measured at a definite spatial scale, which is conceptually equivalent to $P_B^{(\mathrm{Cantor})}(w)$ of our case. We derive $P_B^{(\mathrm{Cantor})}(w)$ in the Appendix, and it turns out to follow a logarithmic normal distribution as a distribution in Kolmogorov's theory,

$$P_B^{(\mathrm{Cantor})}(w) \sim \frac{1}{w} N_{(0,n\sigma^2)}(\ln w), \qquad (n \to \infty), \tag{16}$$

where $N_{(\mu,\sigma^2)}(x) = \frac{1}{\sqrt{2\pi}\sigma} e^{-\frac{(x-\mu)^2}{2\sigma^2}}$ and σ^2 is the variance of the logarithm of the scales to generate a multi-scale Cantor set and n is the number of steps to produce the set. Thus for a multi-scale Cantor set, $P_B^{(\mathrm{Cantor})}(w)$ becomes broader for large n and does not converge to a normalizable distribution. This contrasts with the behavior of $P_B(w)$ for the Fibonacci model.

As shown in the Appendix, we can modify the construction of a multi-scale Cantor set so that $P_B^{(\mathrm{Cantor})}(w)$ has a constant variance by including a finite size correction to the scales at each splitting step. When we write the width of a band produced at step k as $w_k = e^{-k\epsilon_k}$, ϵ_k would receive a correction proportional to $\frac{\ln k}{k}$. Then

$$P_B^{(\mathrm{Cantor})}(w) = \frac{1}{w} N_{(0,\sigma^2)}(\ln w). \tag{17}$$

A graph for a logarithmic normal distribution is shown in Fig. 6. At the origin, the logarithmic normal distribution approaches zero faster than power law. Also at the tail, it does not decay at an exponential rate. Thus, the behavior of $P_B^{(\mathrm{Cantor})}(w)$ of this multi-scale Cantor

set with the finite size corrections shows differences from those of the Fibonacci model.

These differences may be rooted in the degree of self-similarity. The multi-scale Cantor sets are genuinely self-similar : the same splitting procedure is applied to every interval at each step. This leads to a logarithm normal contribution. On the other hand, the splitting of the energy levels of the Fibonacci model is different for each band and it has different scales for different bands [11, 15]. In [15], it has been observed that numerical values of scales of the band's center coincide with eigenvalues of the linearized KKT map at the hyperbolic points of the corresponding periodic orbit and the splitting of the bands is explained by the Smale's horseshoe structure. This observation can be applied to other periodic orbits corresponding to other bands. Then, at least, some subsets of the bands are self-similar and should satisfy the band-width distribution like the multi-scale Cantor sets. Still a finite number of periodic orbits only lead to the sum of logarithmic normal distributions and cannot explain fully the behavior of the Fibonacci model.

Then our comparison implies that, to understand the behavior of $P_B(w)$ of the Fibonacci model by the language of dynamical system, it is necessary to include finite size corrections as well as an infinite number of periodic orbits. Such a fine structure of fractal is not taken into account in multifractal analysis of [7], which characterizes fractal objects by the statistical distribution of scales. As proved in [16], the energy spectra of the Fibonacci model belong to a class of a general Cantor set. Thus they belong to a different class of Cantor sets to the multi-scale Cantor sets.

We also compare the results for the gap distribution. The gap distribution of the multi-scale Cantor set follows an inverse power law near the origin $s \to 0$

$$P_G^{(\mathrm{Cantor})}(s) \sim s^{-\delta}, \qquad \delta = D_H + 1, \tag{18}$$

where D_H is the Hausdorff dimension. This is because the length of gaps of a multi-scale Cantor set is directly related to the length of the removed elements since the bands and gaps are complementary in a fixed interval. Although the Fibonacci model have an inverse power law like Eq.(18) for the gap distribution, the relation $\delta = D_H + 1$ does not hold for the Fibonacci model because of the value of the Hausdorff dimension ~ 0.685 [14]. This discrepancy is due to the splitting of the energy levels as observed in Fig. 1: the energy levels of the Fibonacci model have fluctuating endpoints, and the bands and the gaps are not complementary of a fixed interval, and hence have different scaling properties. On the other hand, for the Harper model, the numerical results of [9, 10] seem to sustain the relation $\delta = D_H + 1$. From the same reasoning, there seems to exist no explanation for it actually.

V. CONCLUSION

Spectral properties of the Fibonacci model are examined numerically by using the Kohmoto-Kadanoff-Tang map. We investigated the band-width distribution $P_B(w)$ and the gap distribution $P_G(s)$. We find a power law $P_B(w) \sim w^{\alpha}$ near the origin and an exponential decay $P_B(w) \sim e^{-\beta w}$ toward infinity ($\alpha, \beta > 0$). Also $P_G(s)$ diverges with an inverse power law $s^{-\delta}$ near the origin ($\delta > 0$). The indices turn out to depend on the coupling constants through the constant of motion in the Kohmoto-Kadanoff-Tang map.

We compare the band-width distribution $P_B(w)$ and the gap distribution $P_G(s)$ of the Fibonacci model with those of multi-scale Cantor sets. As the distribution of the "band" widths $P_B^{(\mathrm{Cantor})}(w)$ for multi-scale Cantor sets always obeys a logarithmic normal distribution, the behavior of $P_B(w)$ is rather different from that of $P_B^{(\mathrm{Cantor})}(w)$. Also, while the distribution of the "gaps" $P_G^{(\mathrm{Cantor})}(s)$ of the multi-scale Cantor sets is an inverse power law $s^{-\delta}$ near the origin ($\delta > 0$) and there is the relation between the index δ and its Hausdorff dimension, the relation does not hold for the Fibonacci model. Thus the critical level statistics is useful to quantify differences between the energy spectra of the Fibonacci models and multi-scale Cantor sets which are hidden in the language of multifractal analysis.

Acknowledgments M.N. would like to thank Y. Takada for discussion. The research of M.N. is supported by JSPS fellowship (No.0206911). K.I. has benefited from the Grand-in-Aid for Science(B), No.1430114 of JSPS.

APPENDIX: DISTRIBUTIONS FOR THE MULTI-SCALE CANTOR SETS

The general definition of a Cantor set is a closed set with no isolated points and whose complement is dense. Here we restrict ourselves to the so-called multiple-scale Cantor sets. A multi-scale Cantor set is a set which is obtained by the following procedure : we transform the interval $I = [0, 1]$ into a finite number of subintervals with definite scales and apply the same transformation to subintervals, and the limit set is called a multi-scale Cantor set.

A standard example is the classical Cantor set : We split an interval into three equal pieces and remove the middle one. Two remaining intervals are $[0, \frac{1}{3}]$ and $[\frac{2}{3}, 1]$. One can continue the same transformation for these intervals. The number of intervals which we call "band" at step n is given by $N = 2^n$ with length $W = \frac{1}{3^n}$. The removed intervals, which we call "gap", have lengths $S = \frac{1}{3}, \frac{1}{3^2}, \cdots, \frac{1}{3^n}$. As n goes to ∞, we end up with an infinite number of infinitesimal intervals. The Hausdorff dimension of the set is given by $D_H = \frac{\ln N}{\ln \frac{1}{W}} = \frac{\ln 2}{\ln 3}$.

For a multi-scale Cantor set, let n be the number of steps to generate the set and N be the number of bands : $N \sim a^n$ with a number of split intervals a. Let W_i, S_i $(i = 1, \cdots, N)$ be the length of bands and gaps respectively. We normalize W_i so that their mean is equal to 1. The mean of W_i at step n is given by $\overline{W}_n = \frac{1}{N}\sum_{i=1}^{N} W_i$. The normalized band-widths are $w_i := \frac{W_i}{\overline{W}_n}$.

For the Cantor set with one scale described above, $N = 2^n, W_i = 3^{-n}, N\overline{W} = \sum_{i=1}^{N} W_i = \frac{2^n}{3^n}, \overline{W} = \frac{1}{3^n}$ and $w_i = 1$, we have

$$P_B^{(\mathrm{Cantor})}(w) = \delta(w-1). \tag{19}$$

This means that there is no distribution of scaling variables and is readily generalized to a scale other than $\frac{1}{3}$. On the other hand, the gap lengths are $S_i = \frac{1}{3}, \frac{1}{3^2}, \cdots, \frac{1}{3^n}$. The number of the gaps of $\frac{1}{3^k}$ $(k = 1, \cdots, n)$ is 2^k. Thus the distribution of the gaps is given by

$$P_G^{(\mathrm{Cantor})}(s) \sim s^{-\frac{\ln 2}{\ln 3}-1} = s^{-D_H-1}. \tag{20}$$

The power is related to the Hausdorff dimension because the lengths of the gaps consist of those of the band-widths.

Let us next consider a two-scale Cantor set which has two scales $r_1, r_2 > 0$ with $r_1 + r_2 = \rho_0 < 1$. Namely we split an interval into three intervals with length r_1, r_2 and $t = 1-\rho_0$, and remove the interval with the length t. Then we continue the same procedure to the remaining intervals. We put $N = 2^n$, $\rho = \rho_0/2$ and define $\widetilde{x} = x/\rho, \widetilde{y} = y/\rho$.

For the bands, we have

$$W_i = r_1^n, r_1^{n-1}r_2, r_1^{n-2}r_2^2, \cdots, r_1 r_2^{n-1}, r_2^n, \tag{21}$$

where each of them has $\binom{n}{m}$ terms. Then, the mean of the band-widths is given by

$$\begin{aligned} N\Delta &= \sum_m \binom{n}{m} r_1^{n-m} r_2^m = (r_1+r_2)^n = \rho_0^n, \\ \Delta &= \rho^n. \end{aligned} \tag{22}$$

The normalized band-widths are

$$w_i = \widetilde{r}_1^n, \widetilde{r}_1^{n-1}\widetilde{r}_2, \widetilde{r}_1^{n-2}\widetilde{r}_2^2, \cdots, \widetilde{r}_1\widetilde{r}_2^{n-1}, \widetilde{r}_2^n. \tag{23}$$

Since the binomial distribution $\binom{n}{x}$ converges to a normal distribution as $n \to \infty$, when n is taken as a discrete time, x can be regarded as a discrete Brownian motion (a binomial model of it). To get $P_B^{(\mathrm{Cantor})}(w)$ for $n \to \infty$, let us recall the central limit theorem:

[Theorem] (The Central Limit Theorem)

Let X_k be independent stochastic variables following an identical probabilistic distribution. Let $E(X_1) = \mu, Var(X_1) = \sigma^2$. Then

$$\lim_{n\to\infty} \mathrm{Prob}\left[\frac{X_1 + X_2 + \cdots + X_n - n\mu}{\sigma\sqrt{n}} \le x\right] = \Phi(x),$$

$$\Phi(x) = \int_{-\infty}^{x} N_{0,1}(y)dy,\ N_{(\mu,\sigma^2)}(y) = \frac{1}{\sqrt{2\pi}\sigma} e^{-\frac{(y-\mu)^2}{2\sigma^2}}.$$

□

In our case, we define $X_k = \ln\frac{W_k}{W_{k-1}}$ $(W_0 = 1)$. X_k take values $u = \ln r_1, d = \ln r_2$, and $E(X_k) = \frac{u+d}{2}, Var(X_k) = \frac{(u-d)^2}{4}$. Then the central limit theorem applies :

$$\lim_{n\to\infty} \mathrm{Prob}\left[\frac{\ln\frac{W_n}{W_0} - \frac{n(u+d)}{2}}{\frac{1}{2}(u-d)\sqrt{n}} \le x\right] = \Phi(x). \tag{24}$$

This means that $\ln\frac{W_n}{W_0}$ obeys the distribution $N_{(\frac{n}{2}(u+d), \frac{n(u-d)^2}{4})}$. Returning to the normalized variables w_i, we similarly define $x_k = \ln\frac{w_k}{w_{k-1}}$. The band-width distribution is obtained as

$$P_B^{(\mathrm{Cantor})}(w) \sim \frac{1}{w} N_{(0, \frac{n(u-d)^2}{4})}(\ln w), \qquad (n \to \infty). \tag{25}$$

This is a logarithmic normal distribution whose variance increases linearly with n.

The distribution (25) can be generalized to Cantor sets with arbitrary number of scales as long as the mean and the variance of the scales are finite. In this case, the central limit theorem applies. $P_B^{(\mathrm{Cantor})}(w)$ always obeys a logarithmic normal distribution with a variance proportional to n :

$$P_B^{(\mathrm{Cantor})}(w) \sim \frac{1}{w} N_{(0, n\sigma^2)}(\ln w), \qquad (n \to \infty), \tag{26}$$

where σ^2 is the variance of the logarithm of the scales.

To obtain $P_B^{(\mathrm{Cantor})}(w)$ with a definite variance, one can modify the transformation of splitting a interval. For simplicity, we describe it for the two-scale Cantor set. We divide the interval $[0,1]$ into three intervals with lengths r_1, r_2 and $1-\rho_0$ with $r_1, r_2 > 0$, $r_1 + r_2 = \rho_0 < 1$, and remove the interval with the length $1-\rho_0$. We continue the procedure for the remaining intervals but, at step k, we always replace r_1 and r_2 with $r_1(k) = r_1^{\frac{1}{\sqrt{k}} - \frac{1}{\sqrt{k-1}}}$ and $r_2(k) = r_2^{\frac{1}{\sqrt{k}} - \frac{1}{\sqrt{k-1}}}$. When we write the width of a band produced at step k as $w_k = e^{-k\epsilon_k}$ by an exponent ϵ_k, the factor is amount to change ϵ_k by a finite size correction $\frac{1}{2}\frac{\ln k}{k}$. Then the distribution becomes a logarithmic normal distribution with a constant variance:

$$P_B^{(\mathrm{Cantor})}(w) = \frac{1}{w} N_{(0, \frac{(u-d)^2}{4})}(\ln w). \tag{27}$$

This can be readily generalized to the cases with more than two scales, leading to the distribution

$$P_B^{(\mathrm{Cantor})}(w) = \frac{1}{w} N_{(0,\sigma^2)}(\ln w), \tag{28}$$

where σ^2 is the variance of the logarithm of the scales.

For the gap distribution of the multi-scale Cantor sets, the formula $\int_0^s P_G^{(\mathrm{Cantor})}(s')ds' \sim s^{-D_H}$ with their Hausdorff dimension D_H holds generally because the lengths of the gaps are directly connected with those of the band-widths. Thus the gap distribution for the multi-scale Cantor sets is given by

$$P_G^{(\mathrm{Cantor})}(s) \sim s^{-D_H-1}. \tag{29}$$

[1] P. A. Lee and T. V. Ramakrishnan, Rev. Mod. Phys. **57**, 287 (1985).

[2] For a review, see H. Hiramoto and M. Kohmoto, Int. J. Mod. Phys. **B6**, 281 (1992).

[3] S. Aubry and G. André, Ann. Israel Phys. Soc. **3**, 133 (1980).

[4] D.R. Hofstadter, Phys. Rev.**B14**, 2239 (1976).

[5] D.J. Thouless, Phys. Rev.**B28**, 4272 (1983); Commun. Math. Phys. **127**, 187 (1990).

[6] M. Kohmoto, Phys. Rev. Lett. **51**, 1198 (1983).

[7] T.C. Halsey, M.H. Jensen, L.P. Kadanoff, I. Procaccia and B.I. Shraiman, Phys. Rev. **A33**, 1141 (1986); M. Kohmoto, Phys. Rev. **A37**, 1345 (1988).

[8] N. Evangelou and J.-L. Pichard, Phys. Rev. Lett. **84**, 1643 (2000).

[9] Y. Takada, K. Ino and M. Yamanaka, Phys. Rev. **E** in press, [cond-mat/0312650].

[10] K. Machida and M. Fujita, Phys. Rev. **B34**, 7367 (1986); T. Geisel, R. Ketzmerick and G. Petschel, Phys. Rev. Lett. **66**, 1651 (1991).

[11] M. Kohmoto, L.P. Kadanoff and C. Tang, Phys. Rev. Lett. **50**, 1870 (1983).

[12] S. Ostlund, R. Pandits, D. Rand, H.J. Schellnhuber and E. Siggia, Phys. Rev. Lett. **50**, 1873 (1983).

[13] M. Kohmoto and J.R. Banavar, Phys. Rev. **B34**, 563 (1986).

[14] M. Kohmoto, B. Sutherland and C. Tang, Phys. Rev. **B35**, 1020 (1987).

[15] M. Kohmoto and Y. Oono, Phys. Lett. **102A**, 145 (1984).

[16] A. Sütõ, J. Stat. Phys. **56**, 525 (1989).

[17] A.N. Kolmogorov, J. Fluid. Mech. **13**, 82 (1962).